NUMERICAL SIMULATION ON DOWNHOLE FLOW AND TEMPERATURE FIELDS DURING DRILLING WITH NITROGEN JET

by

Chengzheng CAI [a, *], Keda REN [a], Jiangfeng LIU [a], Shuang LIU [b]

a State Key Laboratory for GeoMechanics and Deep Underground Engineering, China University of Mining and Technology, Xuzhou, China
b CNPC Greatwall Drilling Company, Beijing, China

In petroleum engineering, nitrogen drilling is an important technology for building wellbores between surfaces and reservoirs. To uncover the downhole flow field and the change rules of rock temperature during drilling with N2 jet, we constructed a computational fluid dynamics model by coupling the property equations of nitrogen. The flow fields of N2 jet and rock temperature distribution at different times were simulated. Results showed that the high-speed N2 jet can be efficiently generated because of the nozzle acceleration and the impingement effect can be induced during drilling. The temperature of the N2 jet decreased due to the Joule–Thomson effect. This phenomenon suggested that the N2 jet induced additional thermal cracks on the bottomhole rock, which was very beneficial for the improvement of rock-breaking efficiency.

Key words: gas drilling, N2 jet, flow field, temperature field

Introduction

In petroleum engineering, gas drilling is an important unbalanced drilling method and can greatly improve the rate of penetration. Compared with conventional drilling technologies, gas drilling utilizes gas as the drilling fluid [1]. Through this method, underbalanced drilling can be easily realized in a downhole region because of the low density of gas media. In drilling treatment, water-based drilling fluid can cause the clay swelling and water blocking [2,3]. However, the issues of formation damage can be solved perfectly when drilling with gas [4,5]. Thus, this technology has been widely used in tight gas and shale gas reservoirs [6].

In gas drilling, a high-speed jet will be generated when a drilling fluid is injected into a wellbore [7, 8]. Notably, this effect is proportional to the compressibility of the gas [9]. Owing to the Joule–Thomson effect, the temperature of fluid greatly decreases. To uncover the downhole flow field and heat transfer characteristics during drilling with N2 jet, we constructed a computational fluid dynamics model and then solved the continuity, momentum, energy, and heat conduction equations. The flow and temperature fields of N2 and rock were analyzed according to the simulation results.

* Corresponding author. E-mail: caicz@cumt.edu.cn

Model detail

Geometric model and boundary conditions

Figure 1 was a 2-D geometric model for N2 jet drilling was built. This model consisted of the fluid and solid parts. The fluid part contained three regions: nozzle region, downhole region, and annulus region. The solid part referred to the ambient rocks. During N2 jet drilling, the N2 was injected through the drill pipe and then accelerated by the nozzle. As the N2 discharged from the nozzle, the high-speed jet was generated in the downhole region. Then, the N2 jet impinged the bottomhole rock and then flowed out the downhole region through the annulus. In this model, the wellbore diameter was 50.8 mm, the drill pipe diameter was 31.8 mm, the thickness of rock was 30 mm, the distance between nozzle outlet and bottomhole (i.e., standoff distance) was 30 mm, and the nozzle outlet diameter was 6 mm. According to flow principles, the nozzle inlet was set as the pressure–inlet boundary condition, and the annulus outlet was set as the pressure–out boundary condition.

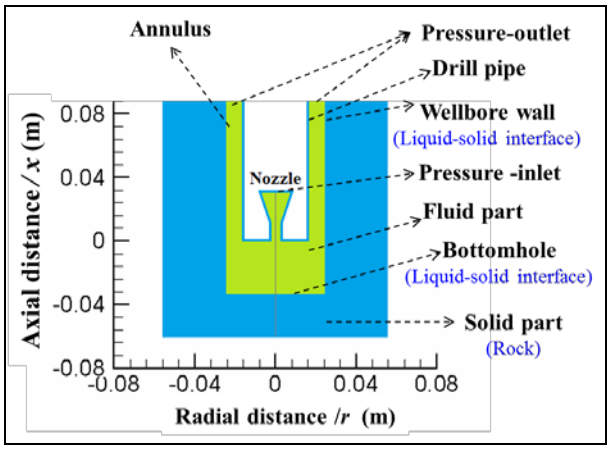

Figure 1. Geometric model and boundary conditions

Governing equations

As the N2 jet is a high-speed flow process, we adopted the k-ε model to consider turbulence closure. The governing equations for the compressible fluid flow in unsteady motion are provided as follows:

For a compressible fluid, the continuity equation can be written as follows [10]:

$$\frac{\partial \rho}{\partial t} + div(\rho \vec{v}) = 0 \tag{1}$$

The momentum equations can be expressed in the cylindrical polar coordinate system because the geometry model had an axisymmetric structure, as follows [10]:

$$\begin{aligned} &\frac{\partial(\rho v_x)}{\partial t} + \frac{1}{r}\frac{\partial}{\partial x}(r\rho v_x v_x) + \frac{1}{r}\frac{\partial}{\partial r}(r\rho v_r v_x) \\ &= -\frac{\partial p}{\partial r} + \frac{1}{r}\frac{\partial}{\partial x}\left[r\mu\left(2\frac{\partial v_x}{\partial x} - \frac{2}{3}(\nabla\cdot\vec{v})\right)\right] + \frac{1}{r}\frac{\partial}{\partial r}\left[r\mu\left(\frac{\partial v_x}{\partial r} + \frac{2}{3}\frac{\partial v_r}{\partial x}\right)\right] + F_x \end{aligned} \tag{2}$$

$$\frac{\partial(\rho v_r)}{\partial t}\frac{1}{r}\frac{\partial}{\partial x}(r\rho v_x v_r)+\frac{1}{r}\frac{\partial}{\partial r}(r\rho v_r v_r)= \\ -\frac{\partial p}{\partial r}+\frac{1}{r}\frac{\partial}{\partial x}\left[r\mu\left(\frac{\partial v_r}{\partial x}+\frac{\partial v_x}{\partial r}\right)\right]+\frac{1}{r}\frac{\partial}{\partial r}\left[r\mu\left(2\frac{\partial v_r}{\partial r}-\frac{2}{3}(\nabla\cdot\vec{v})\right)\right]-2\mu\frac{v_r}{r^2}+\frac{2}{3}\frac{\mu}{r}(\nabla\cdot\vec{v})+p\frac{\vec{v}_z^2}{r}+F_r \quad (3)$$

where Cp is the isobaric specific heat of fluid, Fx and Fr are the components of the body forces, p is pressure, t is time, T is temperature, x is the axial direction, r is the radial direction, $\vec{v}$ is the velocity vector, vx is the axial velocity, vr is the radial velocity, vz is the swirl velocity, ρ is density, μ is the dynamic viscosity, and λ is thermal conductivity.

In the calculation of the temperature field, the governing equations for heat transfer should be included. For a compressible fluid, the energy equation can be expressed as follows [11]:

$$\frac{\partial(\rho T)}{\partial t}+div(\rho\vec{v}T)=div(\frac{\lambda}{C_p}gradT)+S_T \quad (4)$$

In the cylindrical polar coordinate system, the heat conduction equation for rock is as follows [11]:

$$\rho C_p\frac{\partial T}{\partial t}=\frac{1}{r}\frac{\partial}{\partial r}\left(\lambda r\frac{\partial T}{\partial r}\right)+\frac{\partial}{\partial x}\left(\lambda\frac{\partial T}{\partial x}\right)+\dot{\phi}_v \quad (5)$$

where $\dot{\phi}_v$ is heat generation rate, and ST is the term for viscous dissipation. In this work, the heat generation rate was equal to zero.

At solid–fluid an interface, the conjugate heat transfer method was employed [12, 13]. The conjugated boundary conditions were set as follows [11]:

$$T_f\big|_{\text{wall}}=T_s\big|_{\text{wall}},\quad \lambda_f\frac{\partial T_f}{\partial n}\Big|_{\text{wall}}=\lambda_s\frac{\partial T_s}{\partial n}\Big|_{\text{wall}} \quad (6)$$

where Tf is fluid temperature, Ts is solid temperature, λf is fluid thermal conductivity, λs is solid thermal conductivity, and n is the common normal direction of the interface.

N2 property equations

Isobaric heat capacity, density, thermal conductivity, and viscosity were considered. The state equation of Span et al. [14] was used for the evaluation of the density and isobaric heat capacity of nitrogen as follows:

$$p(\delta,\tau)=\rho RT\left(1+\delta(\frac{\partial\alpha^r}{\partial\delta})_\tau\right) \quad (7)$$

$$\frac{C_P(\delta,\tau)}{R}=-\tau^2(\alpha^o_{\tau\tau}+\alpha^r_{\tau\tau})+\frac{(1+\delta\alpha^r_\delta-\delta\tau\alpha^r_{\delta\tau})^2}{1+2\delta\alpha^r_\delta+\delta^2\alpha^r_{\delta\delta}} \quad (8)$$

where α is reduced Helmholtz energy, ao is the ideal gas component of reduced Helmholtz energy, ar is the residual part of reduced Helmholtz energy, R is a gas constant, $\delta = \rho/\rho c$, $\tau =$

Tc/T, ρc is the critical density of nitrogen, and Tc is the critical temperature of nitrogen. The detailed expression of reduced Helmholtz energy can be seen in the reference [12].

The Lemmon and Jacobsen model [15] was used to calculate the viscosity and thermal conductivity. The expression of viscosity equation is as follows [15]:

$$\mu(\rho,T)=\mu_0(T)+\mu_R(\tau,\delta) \tag{9}$$

The functional form for thermal conductivity is given as follows [15]:

$$\lambda(\rho,T)=\lambda_0(T)+\lambda_R(\tau,\delta)+\lambda_c(\tau,\delta) \tag{10}$$

where $\mu 0(T)$ is the viscosity of the dilute gas, $\mu R(\tau, \delta)$ is the residual part of viscosity, $\lambda 0(T)$ is the thermal conductivity of the dilute gas, $\lambda R(\tau, \delta)$ is the residual part of thermal conductivity, and $\lambda c(\tau, \delta)$ is the critical enhancement of thermal conductivity.

The gravity (9.81 m/s^2) was also considered. The properties of the rock were set as follows: density, 2500 kg/m3; isobaric heat capability, 760 J/(kg·K); and thermal conductivity, 2.5 W/(m·K).

Simulation results analysis

Flow field

During the simulation, the boundary conditions were set as follows: the pressure at the nozzle inlet (i.e., the inlet pressure), 18 MPa; pressure at the annulus outlet (i.e., the outlet pressure), 10 MPa; initial temperature, 350 K; and injection temperature, 320 K.

Figure 2 shows the downhole velocity contours of N2 jet at different times. As the high-pressure N2 entered the nozzle, the fluid accelerated rapidly. At the nozzle outlet, the high-speed N2 jet emerged. Owing to the strong shearing effect of N2 jet, the fluid in the downhole region was disturbed. After the high-speed impinged the bottomhole rock, it finally returned to surface through the annulus. For drilling engineering, the flow attached to the bottomhole can remove the rock debris, and the flow inside the annulus can take the debris away.

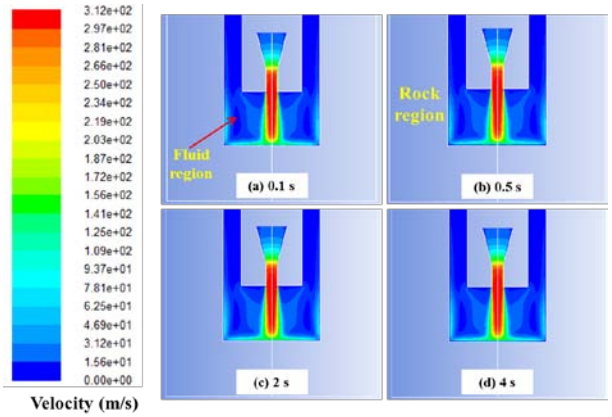

Figure 2. Velocity contours of N2 jet in the downhole region.

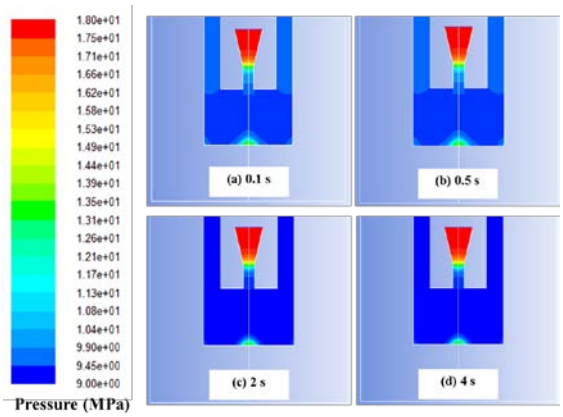

Figure 3. Pressure contours of N2 jet in the downhole region.

The high-speed jet generates a great impingement effect on the bottomhole rock. As shown in

Figure 3, the pressure of N2 decreased continuously when high-pressure N2 flowed through the nozzle. In the cylinder section of nozzle, the pressure decreased slightly. When N2 flowed into the cylinder section of the nozzle, the pressure decreased sharply. Correspondingly, high-speed jet emerged in this region (Figure 2). As the N2 jet reached the bottomhole, the pressure near the jet center increased considerably, thereby generating the impingement effect.

Figure 4 shows the conversion of the velocity and pressure of N2 jet along the axis. At the nozzle inlet, N2 was in a high-pressure and low-speed state. As the N2 entered the conical section of the nozzle, the pressure presented a gradual decrease, whereas the velocity started to increase. At the cylinder section of the nozzle, the pressure decreased quickly. The pressure decreased by 43.12% as the N2 flowed from nozzle inlet to the nozzle outlet. During this process, most of the pressure energy of N2 was transformed into kinetic energy. This transformation explains why the high-speed N2 jet was immediately generated even though it was just discharged from the nozzle. As the jet entered the downhole region and impinged the bottomhole rock, the velocity of the N2 jet decreased, whereas the pressure increased. In this case, partial kinetic energy was transformed into pressure energy, thereby inducing the impingement effect.

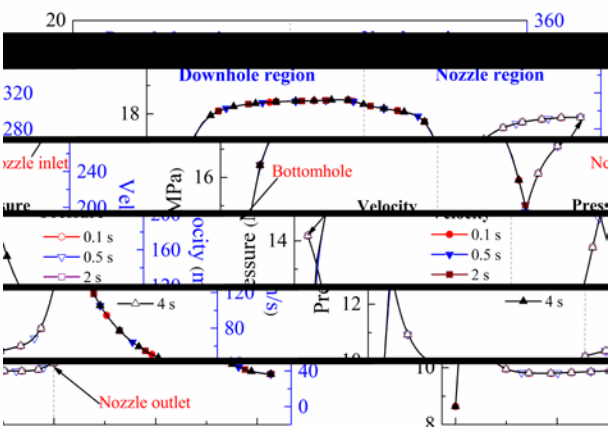

Figure 4. Velocity and pressure distributions of N2 jet along axis

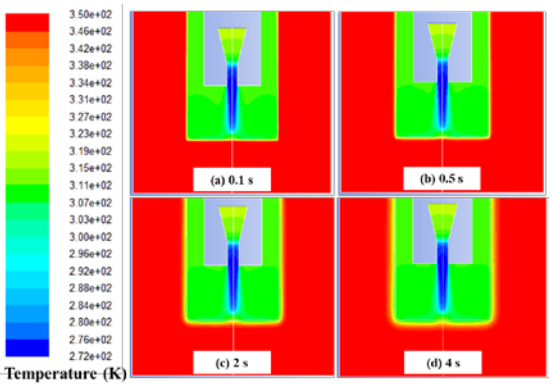

Figure 5. Temperature contours of N2 jet and rock in the downhole region

Temperature field

As mentioned above, the pressure of N2 dropped sharply as it flowed through the nozzle. The length of the nozzle was extremely small, and the velocity of N2 was extremely high. Thus, the heat exchange between N2 and surrounding can be disregarded, and the flow inside the nozzle can be regarded as an insulated process. According to the thermodynamics theory, the Joule–Thomson effect, which presents the decrease in the temperature of the N2 jet, will be generated under this condition. As shown in Figure 5, in the cylinder section of the nozzle, the temperature of N2 was already lower than the injection temperature, indicating that the Joule–Thomson effect was induced. Consequently, as N2 was discharged from the nozzle, the low-temperature jet was generated, as shown in Figure 5. When the low-temperature jet impinged the bottomhole rock, the heat transfer between the N2 jet and rock occurred. From 0.1 s, the cooling region of the rock continuously expanded over time. Drilling with N2 jet induced the thermal cracking apart from the impingement effect.

Figure 6 shows the temperature distributions of jet and rock at different times. From 0.1 s, the temperature of N2 in the downhole region remained unchanged. The heat transfer occurred inside the rock over time. The rock temperature continuously decreased because the bottomhole rock was always subjected to the impingement of the N2 jet. At 2 s, the rock temperature at the jet center position decreased from 350 K (initial temperature) to 316.77 K, presenting a 9.49% decrease. In this case, the thermal tensile stress was approximately 16.62 MPa at the specific rock parameters (Yong's Modulus of 50 GPa and thermal expansion coefficient of 1×10^{-5} K^{-1}). This thermal stress may induce the tensile cracks inside the rock.

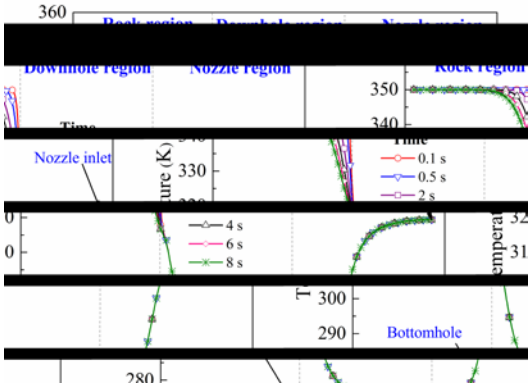

Figure 6. Temperature distributions of N2 jet and rock along axis

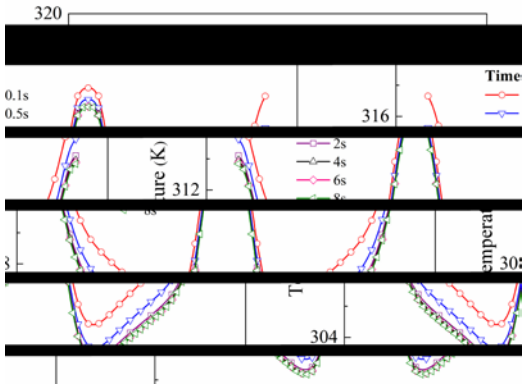

Figure 7. Bottomhole temperature distributions along radial direction

Bottomhole rock temperature distributions

Figure 7 presents the bottomhole rock temperature distribution along the radial direction. The bottomhole temperature decreased over time, and the bottomhole temperature decreased initially and then increased along the radial direction from the well center. At 0.1 s, the temperature was 317.83 K at the well center but 304.78 K at the distance of 8.19 mm from the well center. This phenomenon was also observed in other times. The drop amplitude of the bottomhole rock was closely related to the heat transfer between the low-temperature N2 jet and the rock. Song et al. [16] indicated that this process has two heat loss mechanisms: (1) the direct heat transfer between jet and ambient rock and (2) the heat carried out by flow. The former mainly relies on temperature difference, and the latter is determined by flow rate. As the N2 jet impinged the bottomhole rock, the velocity of the jet attenuated to zero sharply at the well center. Thus, in the region near the well center, heat loss occurred through the direct heat transfer between N2 and the rock. As shown in Figure 8, as the N2 jet impinged the bottomhole rock, the radial unconcentrated flow was induced. From the well center, the radial velocity increased initially and then decreased along the radial direction, and radial velocity reached its maximum value at a certain radial distance. Therefore, the heat carried out by flow played an important role in the heat transfer in the region where the N2 jet had high radial velocity. As shown in Figure 7, the position that was 8.19 mm away from well center had the largest drop amplitude in bottomhole temperature. The high radial velocity in the downhole region facilitated the heat transfer between the N2 jet and rock.

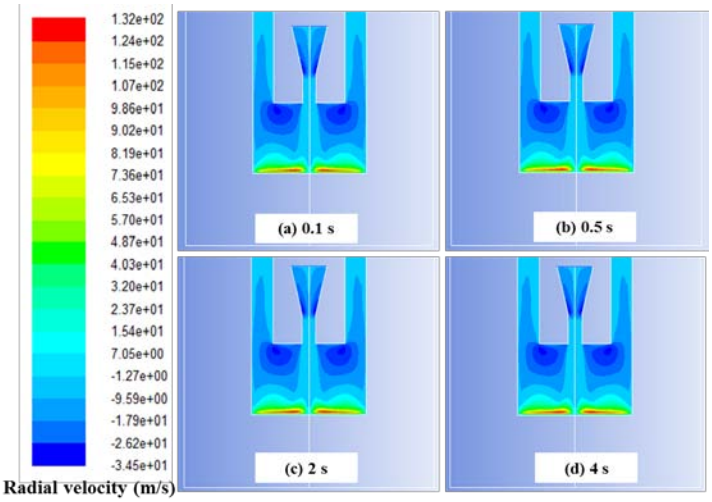

Figure 8. Radial velocity contours of N2 jet in the downhole region

Conclusions

During drilling with N2 jet, the high-pressure N2 was transformed into high-speed jet owing to the acceleration of nozzle. In the downhole region, the high-speed jet generated significant impingement performance on the bottomhole rock. In the cylinder section of the nozzle, the pressure of N2 decreased sharply, and this effect led to the Joule–Thomson effect. Thus, the high-speed N2 jet with low temperature was generated, which absorbed heat from the bottomhole rock and caused a cooling effect on the bottomhole rock. The high radial velocity in the downhole region facilitated the heat transfer between the N2 jet and rock, and thus improved the cooling performance of the bottomhole rock.

Acknowledgments

The authors would like to thank the financial support from the National Natural Science Foundation of China (No. 51604263), the Natural Science Foundation of Jiangsu Province (Nos. BK20160252 & BK20160249), and the State Key Research Development Program of China (No. 2016YFC0600705).

References

[1] Guo, B., Gao, D., New Development of Theories in Gas Drilling, *Petroleum Science*, 10 (2013), 4, pp. 507-514

[2] Wang, H, *et al.*, The Development and Prospect of Supercritical Carbon Dioxide Drilling, *Petroleum Science and Technology*, 30 (2012), 16, pp. 1670-1676

[3] Wang, H., *et al.*, A Feasibility Analysis on Shale Gas Exploitation with Supercritical Carbon Dioxide, *Energy Sources, Part A: Recovery, Utilization, and Environmental Effects*, 34 (2012), 15, pp. 1426-1435

[4] Xue, Y., *et al.*, An elastoplastic model for gas flow characteristics around drainage borehole considering post-peak failure and elastic compaction, *Environmental Earth Sciences*, 77 (2018), 19, pp. 669

[5] Yang, S., *et al.*, The Characteristics of Recycling Gas Drilling Technology, *Petroleum Science*, 9 (2012), 1, pp. 59-65

[6] Chen, X., *et al.*, A New Method for Determining The Minimum Gas Injection Rate Required for Hole Cleaning in Horizontal Gas Drilling, *Journal of Natural Gas Science and Engineering*, 21 (2014), 11, pp.

1084-1090
[7] Huang, Z., *et al.,* Abrasive Water Jet Perforation Experiments under Ambient Pressures, *Atomization and Sprays*, 25 (2015), 7, pp. 617-627
[8] Li, G., *et al.*, Research and Applications of Novel Jet Techniques in Well Drilling, Completion and Fracturing, *Science Foundation in China*, 22 (2014), 2, pp. 68-80
[9] Li, J., *et al.*, The Complexity of Thermal Effect on Rock Failure in Gas-Drilling Shale-Gas Wells, *Journal of Natural Gas Science and Engineering*, 21 (2014), 11, pp. 255-259
[10] Batchelor, G. K., *An Introduction to Fluid Dynamics*, Cambridge University Press, Cambridge, UK, 2000
[11] Tao, W., *Numerical Heat Transfer*, Xi'an Jiaotong University, Xi'an, China, 2001.
[12] Mehra, B., *et al.*, Local Field Synergy Analysis of Conjugate Heat Transfer for Different Plane Fin Configurations, *Applied Thermal Engineering*, 130 (2018), 2, pp. 1105-1120
[13] Xue, Y., *et al.*, Evaluation of the Non-Darcy Effect of Water Inrush from Karst Collapse Columns by Means of a Nonlinear Flow Model, *Water*, 10 (2018), 9, pp. 1234
[14] Span, R., *et al.*, A Reference Equation of State For The Thermodynamic Properties of Nitrogen for Temperatures from 63.151 to 1000 K and Pressures to 2200 MPa, *Journal of Physical and Chemical Reference Data*, 29 (2000), 6, pp. 1361-1433
[15] Lemmon, E. W., Jacobsen, R. T., Viscosity and Thermal Conductivity Equations for Nitrogen, Oxygen, Argon, and Air, *International Journal of Thermophysics*, 25 (2004), 1, pp. 21-69
[16] Song, X., *et al.*, Numerical Analysis on The Impact of The Flow Field Of Hydrothermal Jet Drilling for Geothermal Wells in A Confined Cooling Environment, *Geothermics*, 66 (2017), 3, pp. 39-49

Paper submitted: July 10, 2018
Paper revised: August 25, 2018
Paper accepted: September 22, 2018